doi.org/10.15392/2319-0612.2025.2912
Braz. J. Radiat. Sci., Rio de Janeiro
2025, 13(3A) | 01-18 | e2912
Submitted: 2025-04-28
Accepted: 2025-07-28

A new method for voxelizing mesh phantoms through cross-sectional images

Santos[a*], R. C. M.; Farias[a], W. A. W. A.; Vieiraa[a,b], J. W.; Andrade[b], P. H. A.; Pena[c], J. M. G.; Lima[c], V. J. M.; Lima[d], F. R. A.

[a]Universidade de Pernambuco - Departamento de Energia Nuclear, 50740-540, Recife – PE, Brasil.
[b]Instituto Federal de Pernambuco, 50740-545, Recife - PE, Brasil.
[c]Universidade Federal de Pernanbuco - Departamento de Anatomia, 50670-420, Recife – PE, Brasil.
[d]Centro Regional de Ciências Nucleares do Nordeste, 50740-545, Recife - PE, Brasil.

*Correspondence: raniele.costa@ufpe.br

Abstract: Exposure Computational Models (ECMs) utilize algorithms for ionizing radiation sources and Monte Carlo (MC) codes to simulate radiation transport, its interaction with matter, and to assess the energy deposited in volumes of interest (VOIs) represented by a phantom. The GDN (Numerical Dosimetry Research Group) (CRCN-NE) and the Computational Dosimetry and Embedded Systems Research Group (IFPE) have been developing techniques and software to create anthropomorphic Boundary Representation (BREP) phantoms, which are typically constructed using polygonal meshes due to their better anatomical representation of organs and tissues. To couple BREP phantoms with MC codes, GDN developed a method that converts polygonal meshes into voxels. This process is carried out using the in-house software DIP (Digital Image Processing), which converts mesh.obj files into voxels.sgi (Interactive Graphics Simulations). In this study, a new voxelization technique is presented, utilizing coronal images generated from a mesh phantom using the Blender application and two other tools: DIP (an in-house software) and PHAntoms Manufacturing. Essentially, the method involves using a plane to section the volume containing the phantom in the anteroposterior direction, saving an image of each slice. The total number of images generated is adjusted to reproduce a phantom height of 176 cm, targeting cubic voxels with edge lengths of 0.12 cm, resulting in 272 images. The produced images represent a collection of segmented VOIs with unique identifiers stacked in the DIP, creating an SGI file. The result of this voxelization was compared to the previous GDN method for dosimetric analyses of ionizing radiation.

Keywords: Phantoms, Voxelization, Monte Carlo, Ionizing Radiation.

doi.org/10.15392/2319-0612.2025.2912
Braz. J. Radiat. Scci., Rio de Janeiro
2025, 13(3A) | 01-18 | e2912
Submitted: 2025-04-28
Accepted: 2025-07-28

Um novo método de voxelização de fantomas mesh através de imagens transversais

Resumo: Modelos Computacionais de Exposição (MCEs) utilizam algoritmos de fontes de radiação ionizante e códigos Monte Carlo (MC) para simular o transporte da radiação, sua interação com a matéria e avaliar a energia depositada em volumes de interesse (VOIs) representados por um fantoma. O GDN (Grupo de Pesquisa em Dosimetria Numérica) (CRCN-NE) e Grupo de Pesquisa em Dosimetria Computacional e Sistemas Embarcados (IFPE)) têm desenvolvido técnicas e softwares para criar fantomas antropomórficos Boundary Representation (BREP), os quais normalmente são construídos por malhas poligonais devido a melhor representação anatômica de órgãos e tecidos. Para acoplar os fantomas BREP aos códigos MC, o GDN desenvolveu um método que converte malhas poligonais em voxels. Esse processo é realizado por meio do software in-house DIP (Digital Image Processing), que converte arquivos mesh.obj em voxels.sgi (simulações gráficas interativas). Neste estudo é apresentada uma nova técnica de voxelização a partir de imagens coronais geradas de um fantoma mesh utilizando o aplicativo Blender e os softwares in-house DIP e PHAntoms Manufacturing. Essencialmente, o método consiste em usar um plano para seccionar o volume que contém o fantoma no sentido anteroposterior, salvando a imagem de cada corte. O total de imagens geradas é ajustado para reproduzir a altura do fantoma de 176 cm, visando voxels cúbicos com arestas de 0,12 cm, o que correspondeu a 272 imagens. As imagens produzidas representam uma coleção de VOIs segmentados com identificadores unívocos empilhadas no DIP, criando um arquivo SGI. O resultado dessa voxelização foi comparado com o método anterior do GDN para análises dosimétricas das radiações ionizantes.

Palavras-chave: Fantomas, Voxelização, Monte Carlo, Radiação ionizante.

1. INTRODUCTION

The biological effects of ionizing radiation on the human body are influenced by the absorbed dose and may occur either directly, through damage to the DNA molecule, or indirectly, via the release of radiolysis byproducts. The use of ionizing radiation inherently carries a potential risk: interactions between radiation and human tissues or organs may result in biological damage or even the destruction of irradiated structures. Although low radiation doses, such as those used in diagnostic medical imaging, are generally considered safe and clinically justified due to their diagnostic benefits, several studies suggest that there may still be associated risks resulting from radiation-induced damage. Higher radiation doses, such as those used in radiotherapy, can lead to severe adverse health effects, including irreversible cellular damage, genetic mutations, and a significantly increased risk of cancer. Therefore, a careful evaluation of the benefit-to-risk ratio, whether diagnostic or therapeutic, is essential in each clinical scenario. In this context, the radiosensitivity of individual tissues plays a crucial role in determining the effective dose and must be considered [1].

The GDN (Research Group in Numerical Dosimetry, CRCN-NE, and the Research Group in Computational Dosimetry and Embedded Systems, IFPE) has developed Exposure Computational Models (ECMs) that implement algorithms for simulating photon and electron sources. For these types of ionizing radiation, the equivalent dose in the volumes of interest (VOIs) is equal to the absorbed dose. Since direct measurement of absorbed dose in human VOIs is not feasible, ECMs have emerged as essential tools for assessing equivalent dose distributions, which are necessary to estimate the effective dose. These models enable the simulation of diverse exposure scenarios, the evaluation of potential radiation effects on human tissues, and the optimization of radiological protection measures. By coupling radiation source simulators with voxelized phantoms, robust Monte Carlo (MC) codes

simulate the transport of radiation, its interaction with the VOIs, and the resulting energy deposition within them [2].

Currently, the GDN employs mesh-based modeling techniques to create anthropomorphic phantoms and has developed methodologies to convert these 3D geometries into voxel representations. In 2018, the GDN introduced a specific voxelization technique to convert mesh.obj phantoms into voxels.sgi format, implemented in the in-house software DIP (Digital Image Processing) [3]. This same voxelization method was reused in 2020, demonstrating its robustness and ongoing applicability in subsequent research projects [4].

Voxelized phantoms created using Blender have been documented in studies published by Cassola et al. [5, 6, 7, 8] and Lima et al. [9]. The voxelization technique implemented in Blender is based on the methodology described by Cassola in 2011 [11], where anatomical structures were segmented into coronal slices using Boolean intersection with a plane and subsequently reconstructed using the ImageJ software [12].

In the present study, the MARTIN mesh phantom (Male Adult with macRo circulaTion and lymphatIc vessels phaNtom) [13] was voxelized using the Blender application. Additionally, two in-house software, DIP and PHAMA (Phantoms Manufacturing) [14], were employed to support the voxelization and processing workflow. The MARTIN phantom, developed by Andrade in 2018, was constructed based on ICRP Publication 89 [15] for reference organ masses and ICRU Reports 44 and 46 [16, 17] for tissue density values. MARTIN includes detailed anatomical structures such as the nervous system, as well as blood and lymphatic vessels.

2. MATERIALS AND METHODS

The hardware and software resources required for this study are available at the Multiuser Laboratory of Numerical Dosimetry (LDN), located at the Research Center of IFPE – Recife Campus. The main workstation used features an Intel® Core™ i7 X990 CPU @ 3.47 GHz, 24 GB of RAM, and a 64-bit Windows 7 Ultimate operating system. The following software applications were installed on this system and used during the study: DIP, Blender (version 2.91.0), the PHAMA add-on, and Microsoft Excel. Additionally, a secondary device, a notebook with a 12th Gen Intel® Core™ i5-1235U processor @ 1.30 GHz, 8 GB of RAM, and a 64-bit Windows 11 operating system, was also employed to support data processing and visualization tasks. For this study, the MARTIN phantom was used (Figure 1). This mesh phantom is available on the GDN website at: https://dosimetrianumerica.org/producoes-cientificas/aulas-2/#. MARTIN represents a male adult in an upright (orthostatic) position and contains 131 volumes of interest (VOIs), embedded within an air-filled parallelepiped.

Figure 1: Front view of the MARTIN mesh phantom.

The voxelization technique, as presented in this work and implemented using Blender [10], is based on the method described by Cassola in 2011 [11].

The complete voxelization process followed 9 steps:

STEP 1: IMPORTING THE PHANTOM

In the main window of the Blender application, the following path was used to import the Martin.obj file: *File* → *Import* → *Wavefront Batch (.obj)*.

STEP 2: CREATING THE INTERSECTION OBJECT AND CAMERA

A "plane" was created and modeled to act as the intersection object along the coronal slicing axis of the phantom. In *Object Properties*, the plane's display mode was changed to *Wireframe*, showing only the mesh edges and allowing visualization of the underlying geometry.

The next step was to insert a camera facing the phantom. With the camera selected, under *Object Data Properties* → *Lens*, the camera type was set to *Orthographic*, and the orthographic scale was configured to 175.5 m. Under *Output Properties* → *Dimensions*, the export resolution was set to 443 pixels in X and 1467 pixels in Y. These configurations are essential for determining the physical size of the phantom during the conversion process. Figure 2 illustrates, in item A), the front view through the camera and the plane modeled in wireframe mode. In item B), a lateral view shows the alignment and positioning of the camera (red object) and the plane (yellow object) in relation to the phantom.

STEP 3: CONFIGURING OUTPUT PARAMETERS

In Viewport Shading mode, the *Material Preview* option was selected to achieve simplified lighting for the scene. In the Output section, the directory for saving the images was defined, and the image format was set to PNG. Additionally, the color depth was changed to 16 bits. In *Render Properties* → *Render Engine* → *Eevee*, the rendering engine was selected, and under the *Film* settings, the *Pixel Filter Size* was set to zero. This step ensures the precise identification of color-coded identifiers applied successively to the VOIs.

STEP 4: ASSIGNING MATERIALS TO EACH STRUCTURE

The next step involved assigning a material to each mesh, corresponding to its respective ID. In the Shading interface, the input material node 'RGB' was applied, and values were defined for the R, G, and B channels. Figure 3 illustrates step 4, showing the application of the RGB node to the mesh representing the stomach content, connected to the material output surface.

Figure 2 : Camera and plane alignment. A) Camera lens view and plane in wireframe mode. B) Lateral view of the alignment and positioning of the camera and the plane relative to the phantom.

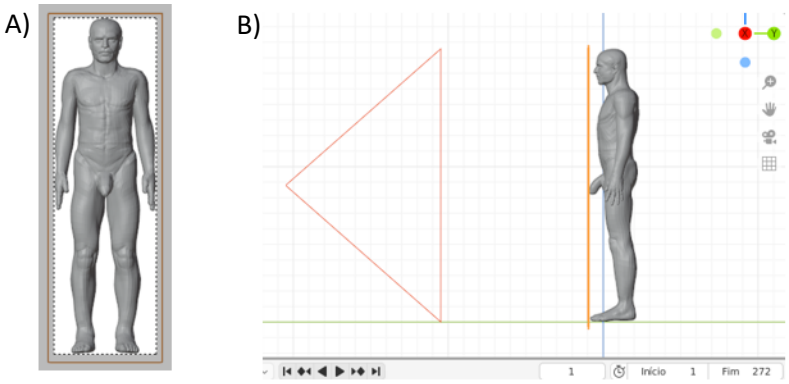

To complete the voxelization of the phantom, 131 distinct materials were defined, each associated with a specific color corresponding to its respective ID. The input values for R, G, and B were assigned to anatomical structures and their respective IDs in the output file. The RGB values range from 0 to 1, which corresponds to an 8-bit grayscale scale (0 to 255 levels). Table 1 presents the list of 131 RGB input values for the materials, along with their corresponding structures and IDs in the output file.

Figure 3 : Application of the RGB node to the stomach content mesh.

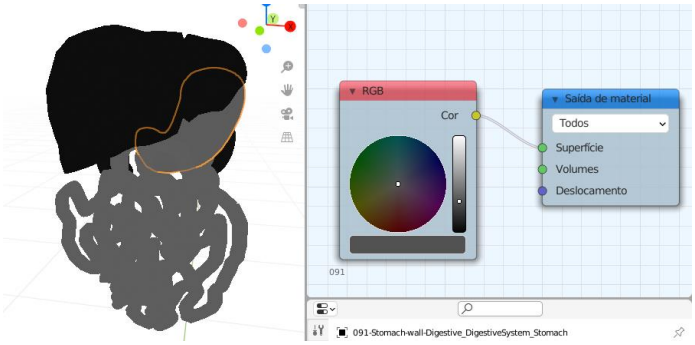

Table 1: List of RGB values associated with the 131 structures and their respective IDs.

RGB	STRUCTURE	ID	RGB	STRUCTURE	ID
	Vacuum	0	0.0265	Blood	48
0.0005	Skin	1	0.027	Penis	49
0.0007	Fat	2	0.028	Abdominal fat	50
0.001	Eyes	4	0.033	Peritoneum	55
0.00125	Eye lenses	5	0.039	Arteries	60
0.0015	Muscle	6	0.045	Lymphatic vessels	65
0.002	Brain (Cerebrum)	7	0.051	Nerves	70
0.0023	Spinal cord	8	0.057	Veins	75
0.0025	Adrenal glands	9	0.08	Gallbladder wall	89
0.0028	Lungs	10	0.085	Stomach wall	91
0.0035	Pancreas	12	0.0885	Small intestine wall	93
0.004	Liver	13	0.092	Colon wall	95
0.0045	Kidneys	14	0.095	Bladder walls	97
0.005	Thymus	15	0.098	Breast fat	98
0.0055	Spleen	16	0.0995	Heart	99
0.0058	Nasal passage	17	0.102	Teeth	100
0.006	Tongue	18	0.105	Mandible	101
0.0065	Oral cavity proper	19	0.108	Skull	102
0.007	Submandibular salivary glands*	20	0.11	Sternum	103
0.0075	Parotid salivary glands*	21	0.112	Ribs	104
0.008	Sublingual salivary glands*	22	0.115	Left clavicle	105
0.009	Pharynx + Larynx	24	0.117	Right clavicle	106
0.0105	Esophagus	26	0.118	Left scapula	107
0.011	Trachea	27	0.12	Right scapula	108
0.0115	Thyroid	28	0.123	Cervical spine	109
0.012	Bronchi	29	0.125	Thoracic spine	110
0.0125	Gallbladder contents	30	0.13	Lumbar spine	111
0.014	Stomach contents	32	0.133	Sacrum	112
0.0155	Small intestine contents	34	0.135	Pelvis	113
0.017	Colon contents	36	0.138	Left humerus	114
0.018	Bladder contents (Urine)	38	0.14	Left radius and ulna	115
0.019	Prostate	39	0.143	Left-hand bones	116
0.02	Testicles	40	0.145	Right humerus	117
0.0205	Lymph nodes	41	0.15	Right radius and ulna	118
0.0215	Soft tissue	42	0.153	Right-hand bones	119
0.022	Periarticular tissue + tendons	43	0.155	Left femur	120
0.025	Gland	46	0.158	Left patella	121

Continuation of Table 1 : Lis of RGB values associated with the 131 structures and their respective IDs.

RGB	STRUCTURE	ID	RGB	STRUCTURE	ID
0.16	Left tibia and fibula	122	0.3	Left foot bones - Spongy tissue	153
0.165	Left foot bones	123	0.305	Right femur - Superior spongy tissue	154
0.168	Right femur	124	0.31	Right patella - Spongy tissue	155
0.17	Right patella	125	0.32	Right tibia and fibula - Spongy tissue	156
0.175	Right tibia and fibula	126	0.325	Right foot bones - Spongy tissue	157
0.178	Right foot bones	127	0.355	Left humerus - Bone marrow	161
0.18	Hyoid bone	128	0.36	Left radius and ulna - Bone marrow	162
0.193	Mandible - Spongy tissue	131	0.37	Right humerus - Bone marrow	163
0.195	Skull - Spongy tissue	132	0.375	Right radius and ulna - Bone marrow	164
0.2	Sternum - Spongy tissue	133	0.38	Left femur - Bone marrow	165
0.205	Ribs - Spongy tissue	134	0.39	Left tibia and fibula - Bone marrow	166
0.21	Left clavicle - Spongy tissue	135	0.4	Right femur - Bone marrow	167
0.215	Right clavicle - Spongy tissue	136	0.41	Right tibia and fibula - Bone marrow	168
0.218	Left scapula - Spongy tissue	137	0.43	Vertebrae - Intervertebral discs	170
0.22	Right scapula - Spongy tissue	138	0.44	Trunk - Articular cartilage	171
0.225	Cervical spine - Spongy tissue	139	0.445	Neck - Thyroid cartilage and epiglottis	172
0.23	Thoracic spine - Spongy tissue	140	0.45	Upper limbs - Articular cartilage	173
0.235	Lumbar spine - Spongy tissue	141	0.46	Ribs - Articular cartilage	174
0.24	Sacrum - Spongy tissue	142	0.47	Head - Ear cartilage	175
0.245	Pelvis - Spongy tissue	143	0.48	Head - Nasal cartilage	176
0.25	Left humerus - Superior spongy tissue	144	0.5	Lower limbs - Articular cartilage	177
0.258	Left radius and ulna - Spongy tissue	145	0.53	Left humerus - Inferior spongy tissue	180
0.26	Left-hand bones - Spongy tissue	146	0.55	Right humerus - Inferior spongy tissue	182
0.265	Right humerus - Superior spongy tissue	147	0.58	Left femur - Inferior spongy tissue	184
0.27	Right radius and ulna - Spongy tissue	148	0.6	Right femur - Inferior spongy tissue	186
0.275	Right-hand bones - Spongy tissue	149	0.85	Air within the bronchi	200
0.28	Left femur - Superior spongy tissue	150	0.87	Air within the trachea	201
0.29	Left patella - Spongy tissue	151	0.9	Air within the pharynx and larynx	202
0.295	Left tibia and fibula - Spongy tissue	152	0.93	Air within	203

STEP 5: CONFIGURE THE PARAMETERS FOR THE INTERSECTION OBJECT AND CAMERA MOVEMENT

The fifth step involves animating both the camera and the intersecting plane to move along the entire Y-axis of the phantom at regular intervals, where each animation frame corresponds to a coronal slice of the model. In the Timeline, *keyframes* were set at the beginning (frame 1) and the end (frame 272) of the animation. With the camera and plane selected, the location matrix was keyed to register the initial position by pressing *the 'I' key* → *Location*. Then, the frame was advanced to 272, and the objects were simultaneously translated along the Y axis until they reached the final slice. *The 'I' key* → *Available* option was selected to record this final keyframe and complete the animation. Figure 4 shows the selected camera and plane animated in an anteroposterior motion, traversing the entire length of the phantom. Item 4A shows the initial slice, while item 4B shows the final slice, with the corresponding slice number highlighted by a black rectangle. A total of 272 images were generated to reproduce the full volume of the phantom.

Figure 4 : Camera and plane animation along the Y axis of the phantom. A) Initial slice. B) Final slice.

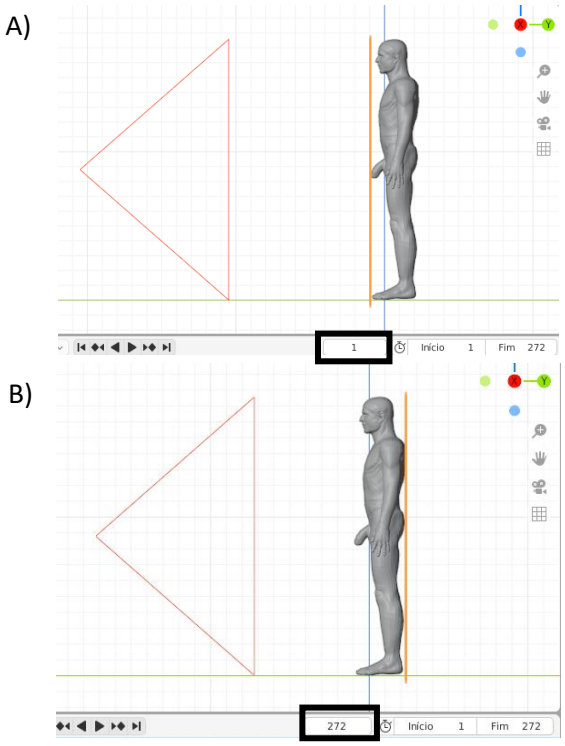

STEP 6: INTERSECTION WITH THE PLANE

The *Boolean* modifier was applied to the VOIs using the fast intersection parameter, with the plane defined as the reference object. This modifier ensures that only the anatomical structures intersecting the plane remain visible in the scene.

STEP 7: GENERATE PHANTOM IMAGE STACK

In the seventh step, five collections were created in Blender, each organized into a separate layer to group anatomically and radiologically relevant structures. The layers were defined as follows: C1 for skin; C2 for muscle, lungs, and peritoneum; C3 for periarticular structures, cortical skull, and abdominal fat; C4 for bronchi, solid organs, walls of hollow organs, spongy skull, and cortical bones; and C5 for air, contents of hollow organs, brain, spongy bones, and blood vessels. Each layer was assigned the appropriate material corresponding to its structural properties. This organization of the meshes is essential for reducing the total computational time and avoiding processing errors during the voxelization procedure. Figure 5 illustrates the structural distribution across the five layers.

Figure 5: Organization of the MARTIN meshes. C1) Skin. C2) Muscles, lungs, and peritoneum. C3) Cortical skull, periarticular, and abdominal fat. C4) Bronchi, solid organs, walls of organs with cavities, spongy skull, and cortical bones. C5) Air, contents of organs with cavities, brain, spongy bones, and vessels.

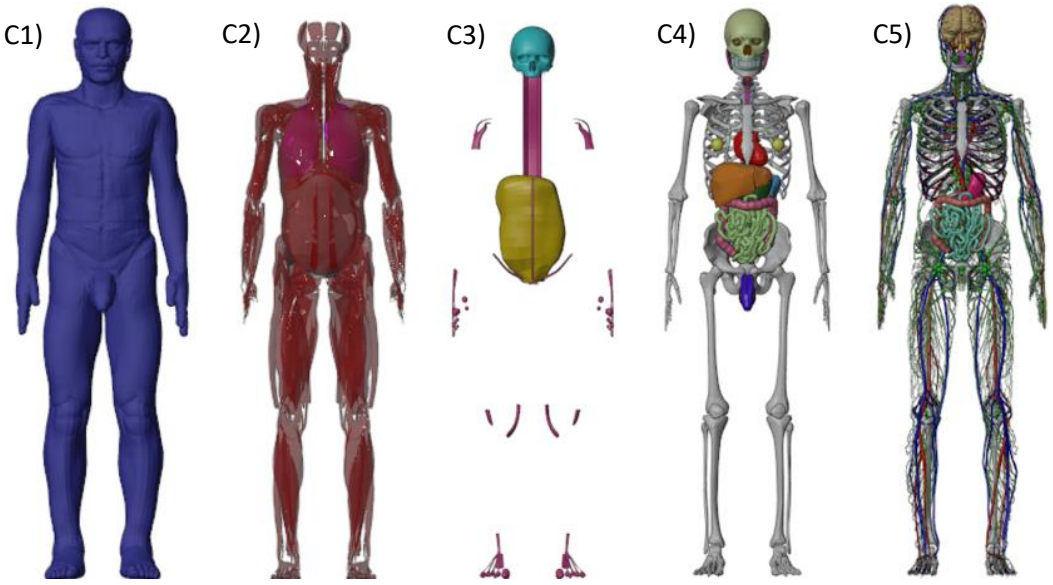

For the voxelization process, the plane was hidden in the viewport to ensure that its edges did not interfere with the generated images, and the renderings were performed in the Shading interface. To initiate Step 8, the menu path *View* → *Viewport Render Animation* was followed. This procedure executed the voxelization, and the resulting images were automatically saved in the pre-specified directories.

Some images generated during the voxelization process exhibited mesh defects, requiring replacement of the faulty slice. To correct these errors, the *Voxel Size* parameter of the problematic mesh must be adjusted through the *Remesh* modifier. This adjustment reorganizes and repairs the mesh structure. Figure 7 shows the mesh failure in the veins on slice 129, marked by a red circle. The black rectangles highlight the voxel size adjustment applied to the structure. In item A), the *Voxel Size* is 1 mm, where the defect is visible. In item B), the *Voxel Size* was changed to 2 mm, effectively correcting the failure.

To ensure proper operation of the modifiers, a specific order must be followed: the *Remesh* modifier must be positioned above the *Boolean* modifier. After adjusting the mesh, the corrected slice is rendered again, replacing the previous version with the applied fix.

Figure 6: Mesh correction in the slice. A) Mesh error in the artery. B) Change in *Voxel Size* to correct the error.

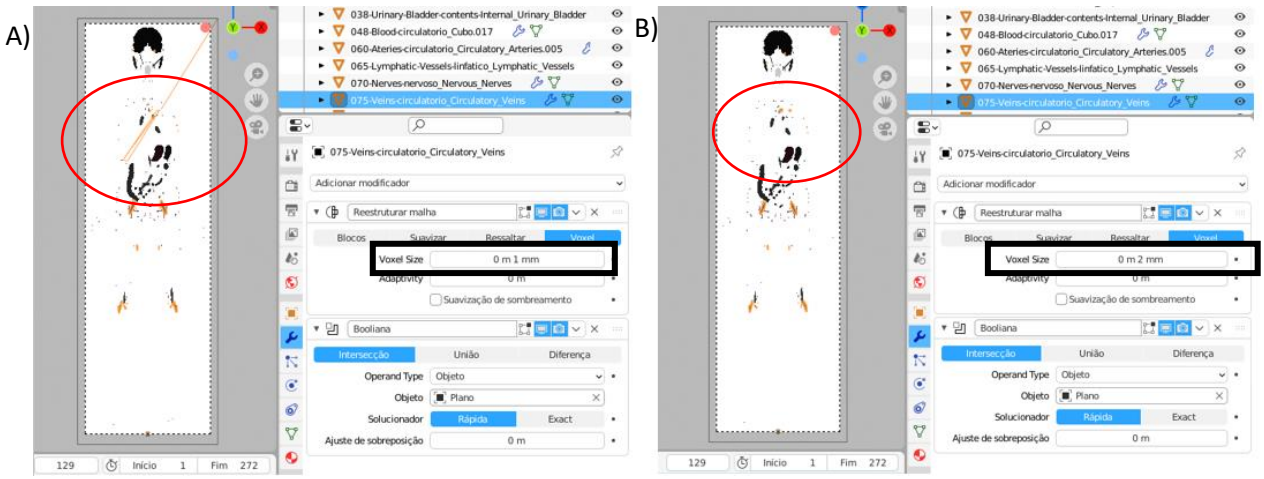

STEP 8: IMAGE CONVERSION

The image stacks resulting from the renderings were converted using DIP into the SGI format, generating five files. Specifically, for the skin file, within the DIP interface, the following menu path was followed: *Studies* → *Phantom Construction* → *Phantom Manipulation in FANTOMAsSGI* → *Deterministic Adjustments* → *Create Organ Content by Replacing Internal Voxels*. The internal ID was set to 2, corresponding to adipose tissue, while the contour ID was set to 1, representing the skin. Thus, this step resulted in the creation of a file containing two tissue types: skin (ID 1) and adipose tissue (ID 2).

STEP 9: FINALIZING VOXELIZATION IN DIP

The addition function in DIP enabled the merging of these image stacks, applying the following rule for intersections: when different non-zero IDs overlap, the one representing the smaller VOI is selected. This process resulted in a new file named MARTIN.sgi. This step allows volumetric reconstruction from the coronal slices, where each slice contributes to the formation of the three-dimensional model.

The phantom produced in this study was compared with the voxelization result obtained through DIP [3] using the linear correlation coefficient.

3. RESULTS AND DISCUSSIONS

The voxelization method implemented in Blender successfully generated the voxelized version of the MARTIN phantom using the same list of IDs applied to other phantoms integrated into the MC EGSnrc code [18] by the GDN. The organ mapping, essential for this process, was performed through a direct correspondence between RGB values and the final IDs, as detailed in Table 1, ensuring the correct assignment of each ID to the respective VOI. Figure 7 shows the voxelized MARTIN phantom reconstructed in ImageJ, displayed in three planes: sagittal, coronal, and transverse.

The comparison between the voxel distributions of the VOIs in the MARTIN phantom voxelized by Blender and that voxelized by DIP revealed a high degree of agreement, with a linear correlation coefficient of 0.9967, indicating an equivalent distribution. This strong correlation suggests that both voxelization approaches yield equivalent spatial distributions, thereby supporting the reliability and consistency of the methods.

Figure 8: Voxelized MARTIN phantom. A) Sagittal section. B) Coronal section. C) Transverse section.

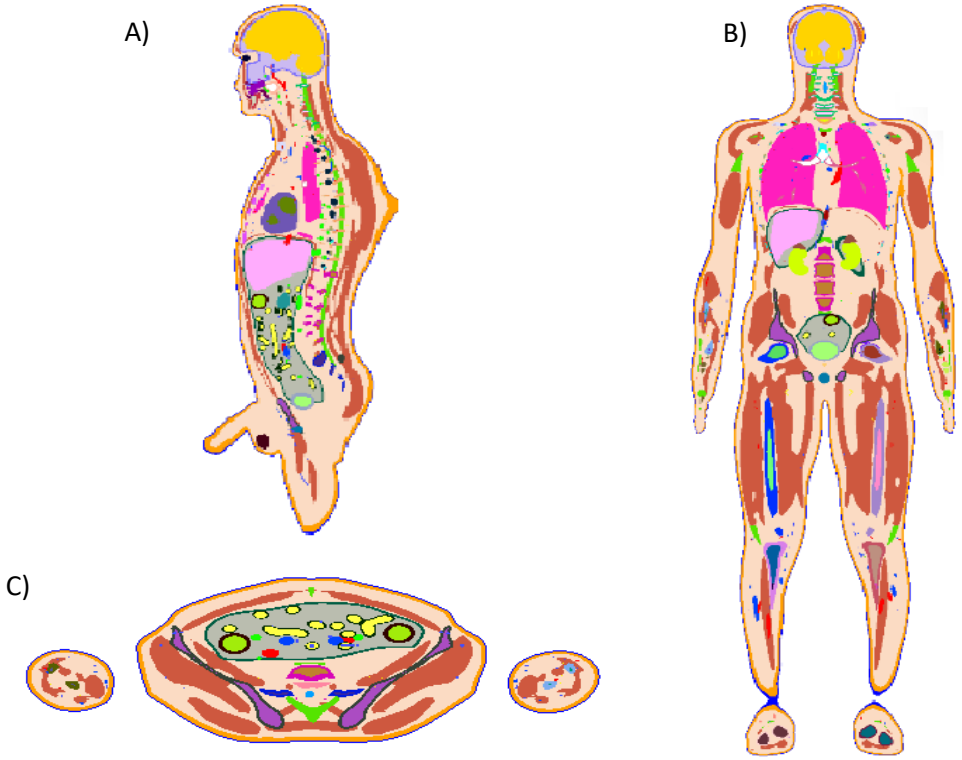

The previous voxelization method developed by GDN, described by Vieira et al. (2018) [3] and applied by Andrade et al. (2020) [4], was based on the DIP software. This method operates directly on the coordinates of mesh vertices and faces, requiring a series of pre-processing steps including exportation and format conversion. Moreover, it imposes strict topological requirements: all meshes must be fully closed to ensure accurate volume filling. Any imperfections, such as open edges or non-manifold geometries, can compromise or entirely prevent voxelization.

The method presented in this work overcomes these limitations by:

1- Optimized workflow: Conducting most of the process within the same modeling environment, eliminating the need for intermediate file conversions, using a vector slicing system instead of direct vertex mapping.

2- Robustness with imperfect meshes: The main advantage of this method is its ability to process meshes with defects. The Boolean intersection technique, combined with Blender's Remesh modifier, ensures that structures with modeling issues (open meshes) are voxelized accurately.

3- Automatic filling: The internal filling of the VOIs occurs automatically during the rendering of each slice in Blender, which interprets the objects as solids, thus eliminating the filling step required in the previous method that depended on mesh integrity.

4- ID consistency: IDs are assigned and provided via RGB values from the start and correspond directly to those already established for dosimetry in the MC EGSnrc code, avoiding the need for ID remapping at the end of the process.

This method shares similarities with the methodology of Cassola et al., who also employed Blender for voxelizing the FASH and MASH phantom couples [5], the supine posture versions FASH2 and MASH2 [6], eighteen male and female phantoms representing different mass percentiles [7], and newborn phantoms [8]. Subsequent works, such as those by Lima et al. [9] using pediatric phantoms, followed a similar approach.

In both methods, the skin is generated as a post-processing step by reassigning voxels on the surface, except for the eyes. Both methods use layered voxelization of structures to prevent overlap.

Cassola's method [11] employs five nodes to define materials for obtaining IDs, while the present method uses only two nodes for this purpose, which suffices to provide a direct correspondence table between RGB values and the final IDs (Table 1).

While Cassola used ImageJ and custom plugins for 3D phantom reconstruction from images, the workflow presented in this article finalizes the merging of layers and the generation of the final file using DIP software, maintaining integration with tools already established by GDN.

4. CONCLUSIONS

Voxelization is a crucial process for converting anatomical models into discrete three-dimensional representations, enabling their use in computational simulations, such as ionizing radiation dosimetry. From this work onward, the GDN offers two methods for mesh phantom voxelization: via Blender or DIP, allowing users to choose the method most suitable for their application.

The voxelization implemented using Blender did not present issues identified in the previous method employed by GDN, such as overlaps between small structures. Furthermore, it ensures that all phantom meshes are voxelized, since the application of the Boolean modifier resolves modeling defects. This approach also optimizes the voxelization process, as most of the procedure is performed directly within Blender, making the process more efficient.

ACKNOWLEDGMENTS

The authors would like to thank FACEPE, IFPE, and CNPq for the financial support provided.

REFERENCES

[1] COSTA, Y. A. P., DO VAL IETSUGU, M., BOLOGNESI, L. Efeitos biológicos da radiação e síndrome aguda das radiações. Tekhne e Logos, Florianópolis, v. 15, n. 1, p. 121-136, 2024.

[2] YORIYAZ, Hélio. Método de Monte Carlo: princípios e aplicações em Física Médica. Revista Brasileira de Física Médica, São Paulo, v. 3, n. 1, p. 141-149, 2009.

[3] VIEIRA, J. W., CABRAL, M. O. M., ANDRADE, P. H. A., NETO, V. L., LIMA, V. J. M., LIMA, F. R. A. (2018). Uso do software DIP para voxelização de fantomas mesh. PROTEÇÃO CONTRA RADIAÇÕES NA COMUNIDADE DOS PAÍSES DE LÍNGUA PORTUGUESA, p. 27.

[4] ANDRADE, P. A., VIEIRA, J. W., OLIVEIRA, V. R. S., VELOSO, R. J. B., LIMA, F. R. A. Um método para voxelização de geometrias 3D de malhas. Brazilian Journal of Radiation Sciences, São Paulo, v. 8, n. 1A (Suppl.), p. 1-12, 2020.

[5] CASSOLA, V. F., LIMA, V. J. M., KRAMER, R., KHOURY, H. J. FASH and MASH: female and male adult human phantoms based on polygon mesh surfaces: I. Development of the anatomy. Physics in Medicine & Biology, v. 55, n. 1, p. 133, 2009.

[6] CASSOLA, V. F. KRAMER, R., BRAYNER C., KHOURY, H. J. Posture-specific phantoms representing female and male adults in Monte Carlo-based simulations for radiological protection. Physics in Medicine & Biology, v. 55, n. 15, p. 4399, 2010.

[7] CASSOLA, V. F. et al. Standing adult human phantoms based on 10th, 50th and 90th mass and height percentiles of male and female Caucasian populations. Physics in Medicine & Biology, v. 56, n. 13, p. 3749, 2011.

[8] CASSOLA, V. F., MILIAN, F. M., KRAMER, R., LIRA, C. A. B. O., KHOURY, H. J. Development of newborn and 1-year-old reference phantoms based on polygon mesh surfaces. Journal of Radiological Protection, v. 33, n. 3, p. 669, 2013.

[9] LIMA, V. J. M., CASSOLA, V. F., KRAMER, R., LIRA, C. A. B. O., KHOURY, H. J., VIEIRA, J. W. Development of 5-and 10-year-old pediatric phantoms based on polygon mesh surfaces. Medical physics, v. 38, n. 8, p. 4723-4736, 2011.

[10] BLENDER FOUNDATION. Blender 2.91.0 Manual de referência. Disponível em: <https://download.blender.org/release/Blender2.91/>. Acesso em: 05 nov. 2024.

[11] CASSOLA, Vagner Ferreira. Desenvolvimento de fantomas humanos computacionais usando malhas poligonais em função da postura, massa e altura. 2011. Tese

(Doutorado) – Programa de Pós-Graduação em Tecnologias Energéticas e Nucleares, Universidade Federal de Pernambuco, Recife, 2011.

[12] IMAGEJ. Version 1.54: National Institutes of Health. Disponível em: <https://imagej.softonic.com.br/>. Acesso em: mar. 2025.

[13] ANDRADE, Pedro Henrique Avelino de. Construção e voxelização de um fantoma mesh masculino adulto com macro circulação e vasos linfáticos. 2018. Tese (Doutorado) – Programa de Pós-Graduação em Tecnologias Energéticas e Nucleares, Universidade Federal de Pernambuco, Recife, 2018.

[14] FARIAS, Whoody Alem Wanderley Araripe. Desenvolvimento de uma plataforma computacional para a geração de fantomas antropomórficos e fontes emissoras de elétrons. 2023. Dissertação (Mestrado em Tecnologias Energéticas e Nucleares) – Departamento de Energia Nuclear, Universidade Federal de Pernambuco, Recife, 2023.

[15] ICRP. Basic Anatomical and Physiological Data for Use in Radiological Protection Reference Values. ICRP Publication 89. Ann. ICRP, v. 32, n. 3-4, 2002.

[16] ICRU - International Commission on Radiation Units and Measurements. Tissue substitutes in radiation dosimetry and measurement. ICRU Report 44. U.S.A., ICRU, 1989.

[17] ICRU - International Commission on Radiation Units & Measurements. Photon, electron, proton and neutron interaction data of body tissues. ICRU Report No. 46. Bethesda: ICRU, 1991.

[18] KAWRAKOW, I.; MAINEGRA-HING, E.; ROGERS, D. W. O.; TESSIER, F.; WALTERS, B. R. B. The EGSnrc Code System: Monte Carlo simulation of electron and photon transport. Technical Report PIRS-701. Ottawa, Canada: National Research Council Canada, 2017.

LICENSE